

## Femur Cross-Section Moments Estimation in Full-Scale PMHS Pedestrian Tests

Eric Song, Jerome Uriot, Pascal Potier, Philippe Petit, Xavier Trosseille, Richard Douard

**Abstract** There are few experimental data in literature relating to femur cross-section moments in full-scale PMHS pedestrian tests. However, these moments are used as injury criteria to evaluate pedestrian protection. This study aimed to provide this type of data. In previous studies by the authors, 15 post-mortem human subject (PMHS) were impacted by four different generic simplified vehicle bucks (two sedans, a SUV and a van). Each PMHS was instrumented with three mono-axis strain gauges on its right femur (impacted before the left femur). To derive the moments in the femur from these strain measurements, three-point bending tests were performed on the femurs isolated from the corresponding PMHS tested. The moment-strain relationship for each strain measurement location was then established for each femur. By applying these relationships to the strains measured in the full-scale PMHS tests, the corresponding cross-section moments on the femur were derived. Finally, by scaling these moments, biofidelity corridors were established for the 50<sup>th</sup> percentile male pedestrian in terms of upper, middle and lower cross-section moments in the femur, and for four vehicle profiles. These corridors will allow assessing biofidelity of human body models, physical dummies and lower extremity impactors.

**Keywords** Biofidelity corridor, Dummy, Human body model, Pedestrian impact, PMHS test.

### I. INTRODUCTION

Development of dummies and human body models (HBMs) requires biofidelity targets for their validation. A series of biofidelity targets was developed in the past, based on body region impactor tests, such as in [1-2]. However, this type of testing does not address interaction between body regions and their effect on the overall pedestrian kinematics, dynamics and injury risk. So, it is necessary to perform full-scale pedestrian-vehicle tests in order to bridge this gap. Kerrigan *et al.* performed a series of full-scale pedestrian-vehicle tests in [3-4]. In these tests, production vehicles were cut just rearward of the B-pillar, vehicle wheels were removed and the front suspension was locked. The vehicle bucks were then mounted to a sled and propelled to impact post-mortem human subjects (PMHS) in a mid-gait stance. These tests provided valuable data relative to pedestrian kinematics and injury risk considering its representativeness of real-world vehicles. However, in order to use these data to assess biofidelity of dummies and HBMs, it is necessary to find the same production vehicle for physical testing, and to get the corresponding numerical vehicle model for computational simulations. This necessity limits, to some extent, the use of these data by a larger community.

Considering the limitations above, the use of a generic simplified vehicle represents a good alternative to perform full-scale pedestrian-vehicle tests and to generate pedestrian impact response biofidelity corridors that are easier to use and duplicate for physical tests and computational simulations. Following such considerations, Forman *et al.* performed a first series of three PMHS tests in 2015, using a generic simplified buck representing a small sedan and an impact velocity of 11.1 m/s [5]. In 2016, Song *et al.* developed an adjustable generic simplified vehicle buck, capable of representing different vehicle profiles, and impacted a series of 11 PMHS with the buck at an impact velocity of 11.1 m/s [6]. Furthermore, they have also developed a generic buck representing the front end of a sedan and performed a series of four PMHS tests with the buck at an impact velocity of 8 m/s [7]. In [6-7], kinematics of the subjects were recorded via high-speed videos and impact forces between the subjects and the bucks were measured via load cells behind each tube. Biofidelity corridors were established in terms of pedestrian kinematics and impact forces between the subjects and the buck. These corridors will allow assessing biofidelity of HBMs, physical dummies and impactors.

E. Song (e-mail: eric.song@lab-france.com; tel: +33 176873642), P. Petit and X. Trosseille are researchers in Biomechanics at LAB PSA Renault in Nanterre, France. J. Uriot and P. Potier are researchers in Biomechanics at CEESAR in Nanterre, France. R. Douard is a Professor of Medicine at Université René Descartes, Paris.

Additional measurements were also made in [6-7] and have not yet been published, among them strains on the femur and the tibia at different locations. These strains were measured via strain gauges on these bones. These measurements would allow: 1) determining at which time the femur and/or the tibia fractured if it occurred, and 2) estimating the cross-section moments in these locations. These moments are being used as injury criteria for the tibia fracture risk assessment by the leg impactor FlexPLI. For the new lower extremity impactor aPLI, currently under development in the framework of the International Organization of Standardization (ISO) the cross-section moments in the femur are used as injury criteria to assess the femur fracture risk. Nevertheless, despite the importance of these metrics, there are few experimental data in literature relating to femur cross-section moments in full-scale PMHS pedestrian tests. Consequently, no biofidelity corridors are available to validate HBMs, pedestrian dummies and impactors in full-scale pedestrian impact configurations.

This paper aimed to estimate the cross-section moments in the femur based on the femur strain measurements in [6-7]. To do this, three-point bending tests were performed on the femurs taken from the corresponding PMHS tested. The moment-strain relationship for each strain measurement location was then established for each femur. By applying these relationships to the strains measured in the full-scale PMHS tests, the corresponding cross-section moments on the femur were derived. Finally, by scaling these moments, biofidelity corridors were established for the 50<sup>th</sup> percentile male pedestrian in terms of upper, middle and lower cross-section moments in the femur, and this for four vehicle profiles.

## II. METHODS

### **Reference PMHS Tests**

This section briefly summarises the reference PMHS tests published in previous papers [6-7], where the rationale behind and more detailed information on these tests can be found.

In [6], 11 PMHS were impacted on their right and in a mid-gait stance by an adjustable generic simplified buck at 11.1 m/s. The buck consisted of four components (Fig. 1): two steel cylindrical tubes screwed on rigid supports in V-form, representing the bumper and spoiler respectively, a quarter of a steel cylindrical tube representing the bumper leading edge (BLE), and a steel plate representing the bonnet. The mechanical behaviour of the bumper and the spoiler was determined not only by that of the cylindrical tubes but also by their interactions with the V-forms. The relative position between these components can be easily adjusted to represent different vehicle profiles. In [6], they were positioned differently to represent three types of vehicle profile: a SUV, a van and a sedan. They were defined in order to be in the middle of the car front shape corridors established by the International Harmonized Research Activities (IHRA) [9]. The reaction forces behind the spoiler, bumper and BLE were measured by means of load cells positioned behind each component (exact locations of the load cells and accelerometers can be found in [6-7]). The masses, as well as their accelerations in front of the load cells, were measured and allowed to compensate the reaction force in order to obtain the impact forces sustained by the pedestrians. The reaction forces under the bonnet were also recorded for the van and sedan configurations, but not for the SUV configuration. In total, 11 PMHS tests were performed with the buck. Table I shows test matrix and characteristics of the PMHS tested. Two types of photo marker were used to track PMHS kinematics: 1) the markers stuck on the cloth surface; 2) the spheres screwed on the PMHS bones. Corridors in terms of time histories and trajectories were constructed for the following markers: Head L, Shoulder L, T1, T4, T12, Sacrum Up, Sacrum Low, Knee R, and Ankle R.

The PMHS were initially positioned in a mid-gait stance, with the right lower extremity back and the left lower extremity forward. They were centred relative to the buck in their anterior-posterior direction, and were orientated to be struck laterally on the right side. Regarding the vertical position of each PMHS versus the buck, a target position was first defined for a 50<sup>th</sup> percentile male pedestrian (M50), represented by the GHBMC M50-PS [8] and positioned according to the positioning guidelines in Society of Automotive Engineers (SAE) J2782 [10]. Then, for each PMHS test the relative position of the BLE and the spoiler with respect to the bumper was proportionally scaled according to the thigh and the leg lengths of the PMHS. The buck, with the scaled relative position between its components, was then used to impact the corresponding PMHS. In this way, the impact positions of the spoiler, the bumper and the BLE on the lower extremities were proportionally comparable between different subjects, and consequently the pedestrian responses were more consistent to construct corridors. Without such scaling, a small subject and a large one would be impacted with an identical buck and,

consequently, the bumper, in the SUV configuration for example, would impact the thigh at a higher level with respect to the knee joint when a small subject was used in place of a large one. The applied scaling allowed to impact the thigh at the same location in terms of normalised thigh length. Similar observations can be made for the BLE and the spoiler, and for the van and sedan configurations.

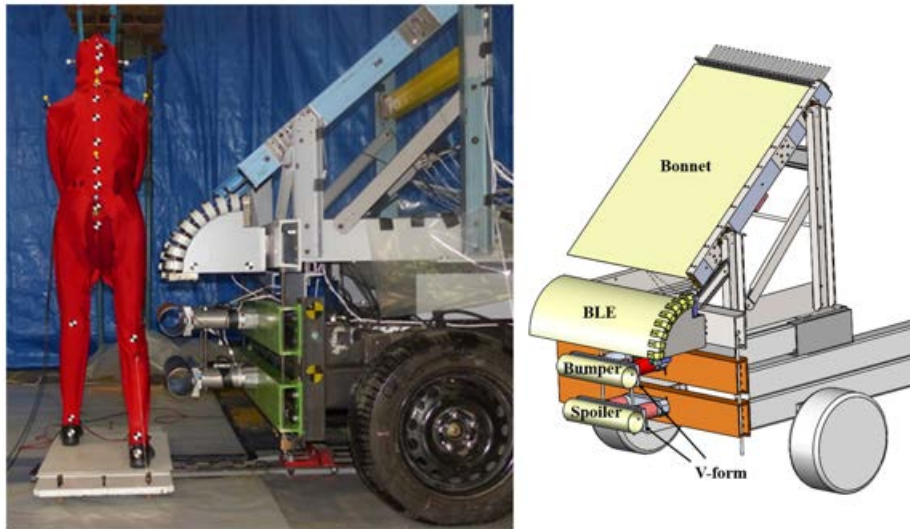


Fig. 1. General view of the LAB pedestrian buck and test setup. Eleven PMHS tests were performed with this buck, adjusted to represent a SUV, a van and a sedan, respectively.

In [7], four PMHS were impacted on their right and in a mid-gait stance by a generic simplified buck at 8 m/s. The buck consisted of three identical steel cylindrical tubes screwed on rigid supports in V-form, representing the BLE, bumper and spoiler of a vehicle, respectively (Fig. 2). The tubes were positioned to represent a mid-size European sedan front-end. All these components were mounted on a pneumatic mini-sled. For each PMHS test the relative position of the BLE and the spoiler with respect to the bumper was proportionally scaled according to the thigh and the leg lengths of the PMHS. The mini-sled, with a total mobile mass of 150 kg, was propelled to 8 m/s to impact four PMHS on their right. After a free race of 650 mm, the mini-sled was progressively stopped via a system of belts with retractor load limiters. The same measurements were recorded in the same way as in the configurations with the impact velocity of 11.1 m/s. Table II shows test matrix and characteristics of the PMHS tested. The PMHS were initially positioned in the same way as in [6].

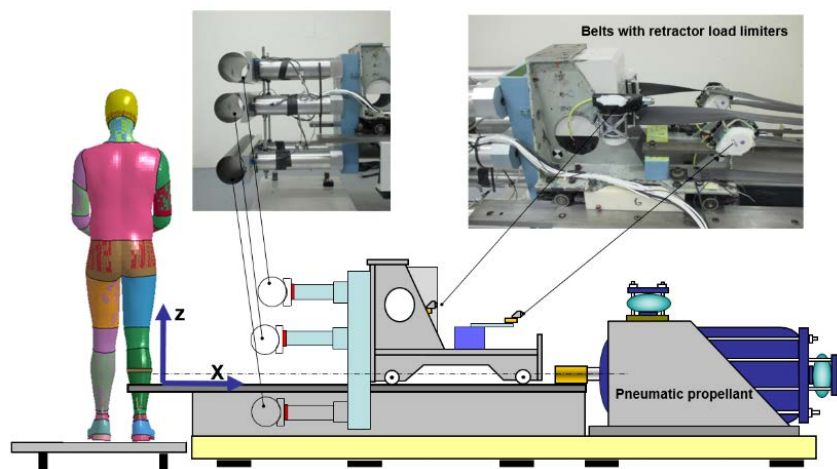


Fig. 2. General illustration of the generic simplified vehicle front-end and the PMHS position represented by the GHBMC 50<sup>th</sup> percentile simplified pedestrian model. Four PMHS tests were performed with this buck.

TABLE I  
TEST MATRIX AND CHARACTERISTICS OF THE PMHS TESTED IN [6]

Test #	Subject #	Configuration	Sex	Mass (kg)	Height (m)	BMI (kg/m <sup>2</sup> )	Age
TIR01	MS697	SUV	M	82	1.63	30.9	62
TIR02	MS698	SUV	M	62	1.63	23.3	82
TIR03	MS699	SUV	M	75	1.66	27.2	87
TIR04	MS700	SUV	M	59	1.60	23.0	81
TIR05	MS701	SUV	M	74	1.56	30.4	80
<i>Average</i>				<i>70</i>	<i>1.62</i>	<i>27.0</i>	<i>78</i>
<i>St. Dev</i>				<i>10</i>	<i>0.04</i>	<i>3.7</i>	<i>10</i>
TIR06	MS712	Van	M	87	1.73	29.1	73
TIR07	MS708	Van	M	62	1.73	20.7	75
TIR08	MS707	Van	M	65	1.71	22.2	64
<i>Average</i>				<i>71</i>	<i>1.72</i>	<i>24.0</i>	<i>71</i>
<i>St. Dev</i>				<i>14</i>	<i>0.01</i>	<i>4.5</i>	<i>6</i>
TIR09	MS711	Sedan	M	64	1.68	22.7	78
TIR10	MS710	Sedan	M	58	1.69	20.3	76
TIR11	MS709	Sedan	M	74	1.63	27.9	66
<i>Average</i>				<i>65</i>	<i>1.67</i>	<i>23.6</i>	<i>73</i>
<i>St. Dev</i>				<i>8</i>	<i>0.03</i>	<i>3.9</i>	<i>6</i>

TABLE II  
TEST MATRIX AND CHARACTERISTICS OF THE PMHS TESTED IN [7]

Test #	Subject #	Configuration	Sex	Mass (kg)	Height (m)	BMI (kg/m <sup>2</sup> )	Age
PCH2210	MS686	3 Cylinders	M	60	178	18.9	83
PCH2211	MS687	3 Cylinders	M	79	171	27.0	77
PCH2212	MS688	3 Cylinders	M	88	178	27.8	71
PCH2213	MS689	3 Cylinders	M	81	173	27.1	87
<i>Average</i>				<i>77</i>	<i>175</i>	<i>25.2</i>	<i>79.5</i>
<i>St. Dev</i>				<i>12</i>	<i>4</i>	<i>4.2</i>	<i>7.0</i>

**Femur strain measurement in buck tests**

Femur strains were measured via three mono-axis strain gauges installed on the medial surface of the right femur according to the following position specifications:

- Superior epiphysis/diaphysis junction;
- Middle of the diaphysis;
- Diaphysis/Inferior diaphysis junction.

Figure 3 provides the average normalised positions (across the 14 full-scale PMHS pedestrian tests) of these three gauges on the right femur from the centre of the femoral head to the distal femur extremity. Table A-II in Appendix provides the normalised locations for all subjects to show variability between subjects.

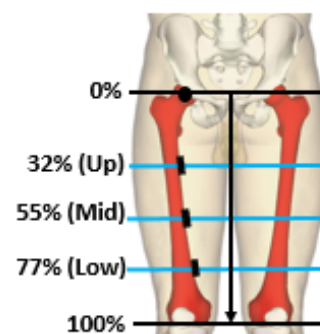


Fig. 3. Locations where strain gauges were installed.

**Bending tests on isolated femurs**

In order to derive the moments in the femur from the above strain measurements, the moment-strain relationship for each measurement position and for each PMHS was necessary. To acquire these data, three-point bending tests were performed on the femurs. These femurs were taken from the PMHS used in the full-scale pedestrian tests, then were further cut just beneath the lesser trochanter to remove the femur neck and head. It

is to be noted that this cut location do not influence the moment-strain relationship in a three-point bending test since this relationship is an intrinsic characteristics of the beam tested (i.e. the femur). Figure 4 shows the three-point bending test setup used. The femur condyle was fixed to the pivoting system by a clamping device. This latter was composed of two pieces: 1) a metal surface in V-form which allowed tightening the femur condyle against the interior surface of the pivoting in Y direction by means of two bolts; 2) a bolt which permitted to block the upward motion of the femur condyle in Z direction. The pivoting system could only rotate around the pivot axis. The other extremity of the femur was maintained by a V-form support in steel, thick enough (8 mm) to avoid its deformation. The height of the support was aligned to the pivot axis so that the lever arm for the friction force was small. This way, the contribution in moment of the friction force was negligible compared to that of the normal component of the support force. A 30 mm diameter full steel cylinder was pushed downwards to load the femur at 50 mm/minute until its complete fracture. Three mono-axis gauges were installed on the medial surface of the femur, at the same locations as in the corresponding full-scale PMHS tests. Strains and loading forces were recorded and filtered at CFC 600. The relative positions between the pivot axis, the loading location, the V-support and the gauges were measured for each test. With these measurements, the moments corresponding to the three gauges' positions were calculated and then related to the strains recorded.



Fig. 4. Three-point bending test setup to acquire moment-strain relationships corresponding to different strain measurement locations.

Table III shows all three-point bending tests performed and corresponding full-scale pedestrian tests. Note that for the 3 Cylinders configuration, two out of four full-scale tests (PCH2211, PCH2212) did not have corresponding three-point bending tests. In fact, the femurs of the two tests were not preserved correctly and could not be used for three-point bending tests. Note also that for two PMHS tests (MS699 and MS711), only tests with the left femurs were performed since their right femurs fractured in full-scale pedestrian tests. These relationships from the left femurs were then used in place of the missing relationships for the right femurs. In order to get some idea about the left and the right femur response difference, the PMHS MS700 and MS701 were tested with their left and right femurs.

TABLE III  
TEST MATRIX OF THREE-POINT BENDING TESTS

Test #	Subject #	Femur	Vehicle configuration	Full-scale pedestrian test #	Remark
PRS549	MS697	Right	SUV	TIR01	
PRS551	MS698	Right	SUV	TIR02	
PRS555	MS699	Left	SUV	TIR03	Right femur fracture
PRS543	MS700	Right	SUV	TIR04	
PRS541		Left	SUV	TIR04	
PRS544	MS701	Right	SUV	TIR05	
PRS542		Left	SUV	TIR05	
PRS546	MS712	Right	Van	TIR06	
PRS547	MS708	Right	Van	TIR07	
PRS552	MS707	Right	Van	TIR08	
PRS556	MS711	Left	Sedan	TIR09	Right femur fracture
PRS550	MS710	Right	Sedan	TIR10	
PRS554	MS709	Right	Sedan	TIR11	
PRS545	MS686	Right	3 cylinders	PCH 2210	
PRS553	MS689	Right	3 cylinders	PCH 2213	

### **Moment vs strain relationship**

Figures A1–A4 in the Appendix show this relationship for each PMHS and each location. It can be observed that these relationships exhibited two characteristics:

- Moment is almost always related to strain linearly in the range of strain between 0% and 0.5%. We hypothesised that this linearity is also true for those femur tests where the peak strain measured did not reach 0.5%;
- The second part of the relationship, in the strain range between 0.5% and 0.8%, can be reasonably represented by a linear relationship.

Based on the above observations, a bilinear elastoplastic model (composed of a first part with an elastic modulus until a strain of 0.5% and a second part with a tangent modulus of 2400 Nm/strain beyond 0.5%) was adjusted to represent the moment vs strain relationship. This representation was necessary to derive the upper femur moment for 4 of 5 SUV tests (detailed explanation is provided in the following section). It is to be noted that this elastic threshold of 0.5% and the constant tangent modulus of 2400 Nm/strain were determined only based on the moment-strain curves given by the three-point bending tests performed in this study. The tangent modulus was obtained by adjusting to minimize the deviation of the model from the experimental relationship in the strain range between 0.0% and 0.8%. Table IV shows the maximum deviation in absolute magnitude and in percentage for each three-points bending test. It was less than 8% in majority of the cases. Only 2 cases (PRS552 Low and PRS554 Low) exhibited larger deviation. However, it is to be emphasized that this model should not be considered in any case as representative of the femur bone behaviour in general.

TABLE IV

MAXIMUM DEVIATION OF A BILINEAR ELASTOPLASTIC REPRESENTATION OF MOMENT-STRAIN RELATIONS FROM EXPERIMENTAL DATA

Moment location	PRS 549	PRS 551	PRS 555	PRS 543	PRS 544	PRS 546	PRS 547	PRS 552	PRS 556	PRS 550	PRS 554	PRS 545	PRS 553
Up	2	1	3	1	2	1	2	1	1	1	1	NA	NA
Mid	5	5	10	8	4	6	11	12	9	6	8	7	4
Low	12	5	3	4	6	6	8	29	1	4	21	4	8
UP	5%	3%	6%	3%	3%	4%	8%	3%	1%	3%	3%	NA	NA
Mid	3%	5%	7%	4%	7%	3%	5%	5%	4%	2%	4%	3%	3%
Low	7%	6%	3%	7%	8%	5%	8%	15%	1%	2%	11%	5%	5%

### **Femur moment calculation for full-scale pedestrian tests**

Based on the characteristics of the strain-moment relationships observed above, femur moments in full-scale pedestrian tests were calculated by the method below.

- When the maximal strain measured in full-scale test at a given location was less than that in the corresponding three-point bending test, the moment-strain relationship obtained from this latter was applied directly to transfer the full-scale test strain curve to the moment curve. These cases are indicated by white cells in Table V.
- When the maximal strain measured in a full-scale test at a given location was larger than that in the corresponding three-point bending test but remained inferior to 0.5%, the elastic modulus obtained from this latter was used to multiply the full-scale test strain curve to get the corresponding moment curve. These cases are indicated by blue cells in Table IV.
- When the maximal strain measured in a full-scale test at a given location was 1) larger than that in the corresponding three-point bending test but 2) superior to 0.5%, and 3) the maximal strain from three-point bending test was superior to 0.5%, the full-scale strain was directly converted to the moment using the strain-moment relationship until it reached the limit of this latter. Beyond this limit, the tangent modulus (calculated using the strain-moment curve in its last 0.05% range) was used to extrapolate the full-scale test moment curve. Only two cases belong to this category and are indicated by yellow cells in Table V.

- Finally, when the maximal strain measured in a full-scale test at a given location was 1) larger than that in the corresponding three-point bending test but 2) superior to 0.5%, and 3) the maximal strain from three-point bending test was inferior to 0.5%, the full-scale moment was derived using a bilinear elastoplastic model, with an elastic modulus calculated from the corresponding three-point bending test until a strain of 0.5% and a tangent modulus of 240 Nm/strain beyond 0.5%. Four cases belong to this category and are indicated by red cells in Table V.

TABLE V

PEAK STRAINS IN THREE-POINT BENDING TESTS AND FULL-SCALE PEDESTRIAN TESTS; FOUR COLOURS DISTINGUISH CASES WHERE FEMUR MOMENTS WERE CALCULATED CASE BY CASE USING DIFFERENT METHODS

Test #	Configuration	3-point bending tests			Whole pedestrian tests			$\lambda_m$
		Low	Mid	Up	Low	Mid	Up	
TIR01	SUV	0.59%	0.76%	0.17%	0.53%	0.83%	0.66%	1.1186
TIR02	SUV	0.49%	0.55%	0.08%	0.41%	0.81%	0.64%	1.4194
TIR03	SUV	0.32%	0.81%	0.15%	0.42%	NA*	0.78%	1.5086
TIR04	SUV	0.43%	1.91%	0.17%	0.41%	0.62%	0.57%	1.7032
TIR05	SUV	0.32%	1.83%	0.30%	0.44%	0.62%	0.46%	1.3200
TIR06	Van	0.44%	2.13%	0.18%	0.38%	0.37%	0.13%	0.9462
TIR07	Van	0.58%	1.11%	0.12%	0.41%	0.41%	0.20%	1.3895
TIR08	Van	0.88%	1.63%	0.30%	0.26%	0.20%	0.20%	1.5086
TIR09	Sedan	0.32%	1.15%	0.18%	0.38%	NA*	0.31%	1.2878
TIR10	Sedan	0.37%	0.84%	0.13%	0.38%	0.55%	0.18%	1.7600
TIR11	Sedan	1.14%	2.22%	0.23%	0.61%	0.64%	0.27%	1.3005
PCH2210	3 Cylinders	0.40%	1.78%	NA**	0.36%	0.54%	0.13%	1.5529
PCH2213	3 Cylinders	0.72%	0.62%	NA**	0.47%	0.20%	-0.21%	1.3069

\* Not provided because of strain measurement drop due to femur fracture in full-scale test, no calculation of corresponding femur moment.

\*\* Not provided because strain range measured at the up position was too small (< 0.05%) to calculate the elastic modulus in the three-point bending test.

### Data scaling and corridors

To establish biomechanical corridors for the 50<sup>th</sup> percentile male, the full-scale test femur moments obtained using the above method were scaled based on the right lower extremity mass of each PMHS:

$$\lambda_m = \frac{m_{50}}{m}$$

$$moment_{scaled} = moment_{unscaled} \times \lambda_m$$

$$time_{scaled} = time_{unscaled} \times \lambda_m^{1/3}$$

where  $m_{50}$  (13.2 kg) is the right lower extremity mass of the 50<sup>th</sup> percentile male,  $m$  is that of the PMHS to scale, and  $\lambda_m$  is the mass scaling factor. The mass scaling factors for the above tests are given in Table IV. Details of their calculations can be found in [6-7].

It is to be noted that three-point bending test data should not be scaled. They were used directly to derive the femur moments in full-scale tests from the corresponding strain measurements.

## III. RESULTS

Time histories of femur strain and femur cross-section moments in full-scale PMHS test are given in Fig. 5 for the SUV configuration, in Fig. 6 for the Van configuration, in Fig. 7 for the Sedan configuration, and in Fig. 8 for the 3 Cylinders configuration. The strain curves correspond to the raw data filtered at CFC 600, no scaling was

performed to normalise the responses to the 50<sup>th</sup> percentile male. The moment curves were derived from strain measurements, filtered at CFC 180 and scaled to the 50<sup>th</sup> percentile male.

For the SUV configuration, the femur fractured in the test TIR03 and led to drop of the strain measurement at its mid position. For this reason, the strain and the moment curves at the mid position were not included in Fig. 5, only four curves being present in the Femur Mid Strain and the Femur Mid Moment graphs. Note that: 1) the strain and the moment peaked quickly, before 10 ms; 2) they also dropped quickly in another 10 ms; 3) the peak strain varied from 0.4% to 0.8% and the peak moment from 200 Nm to 450 Nm.

For the Van configuration, no femur fractured and the curves for all three tests were included in Fig. 6. Note that: 1) the strain and the moment also peaked quickly but slightly delayed when compared to the SUV configuration, between 10 ms and 20 ms; 2) the peak strain varied from 0.2% to 0.4% and the peak moment from 50 Nm to 200 Nm, much less than those in the SUV configuration.

For the Sedan configuration, the femur fractured in the test TIR09 and led to drop of the strain measurement at its mid position. For this reason, the strain and the moment curves at the mid position were not included in Fig. 7, only two curves being present in the Femur Mid Strain and the Femur Mid Moment graphs. Note that: 1) the strain and the moment peaked quite late compared to the SUV and Van configurations, between 25 ms and 30 ms; 2) the peak strain varied from 0.2% to 0.6% and the peak moments from 100 Nm to 350 Nm; 3) the peak strain and the peak moment at the up position was much less important than at the mid and low positions.

For the 3 Cylinders configuration, the strain and the moment curves were given for two out of four full-scale tests. The femurs of the other two tests were not preserved correctly and could not be used for three-point bending tests. For this reason, the strain and the moment curves were included only for two tests in Fig. 8. Besides, the strain range measured at the up position was too small (< 0.05%) to calculate the elastic modulus in the three-point bending test for these two tests, and no femur moment was calculated for the up position. Note that: 1) the strain and the moment peaked also quite late compared to the SUV and Van configurations, around 30 ms; 2) the strain varied from 0.2% to 0.5% and the moment from 100 Nm to 250 Nm for the mid and low locations; 3) the peak strain at the up location was quite small, limited between -0.2% and 0.2%.

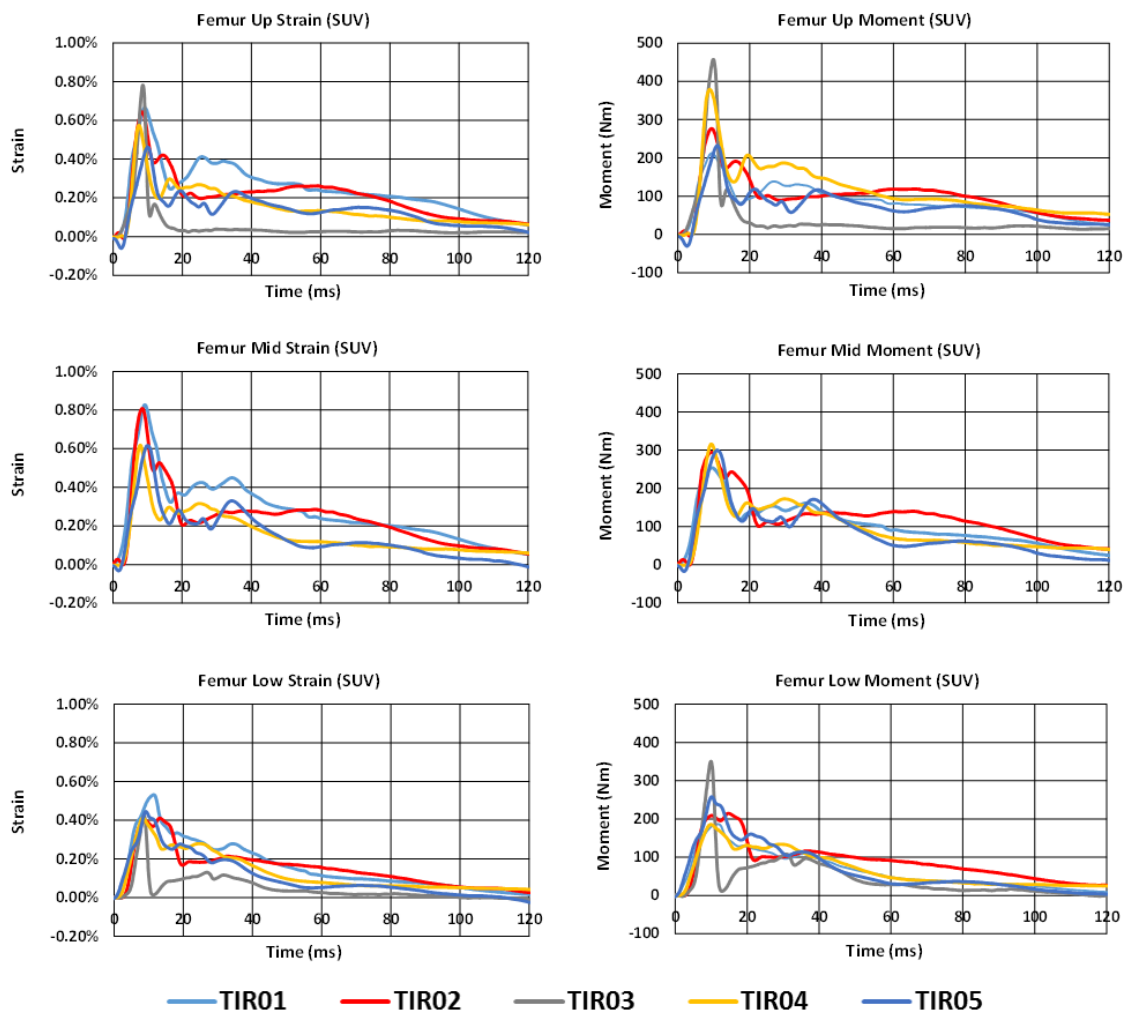


Fig. 5. PMHS responses in the SUV configuration: raw femur strain measurements (left column), femur cross-section moments derived and scaled to the 50<sup>th</sup> percentile male (right column).

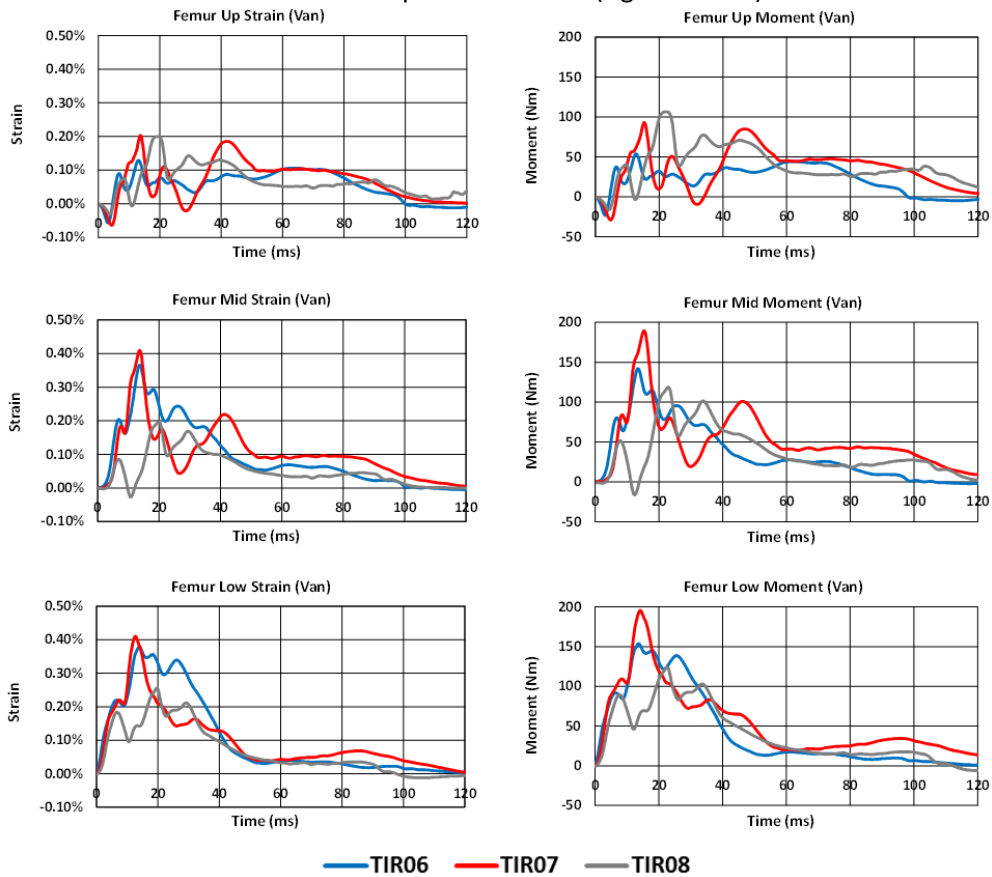


Fig. 6. PMHS responses in the Van configuration: raw femur strain measurements (left column), femur cross-section moments derived and scaled to the 50<sup>th</sup> percentile male (right column).

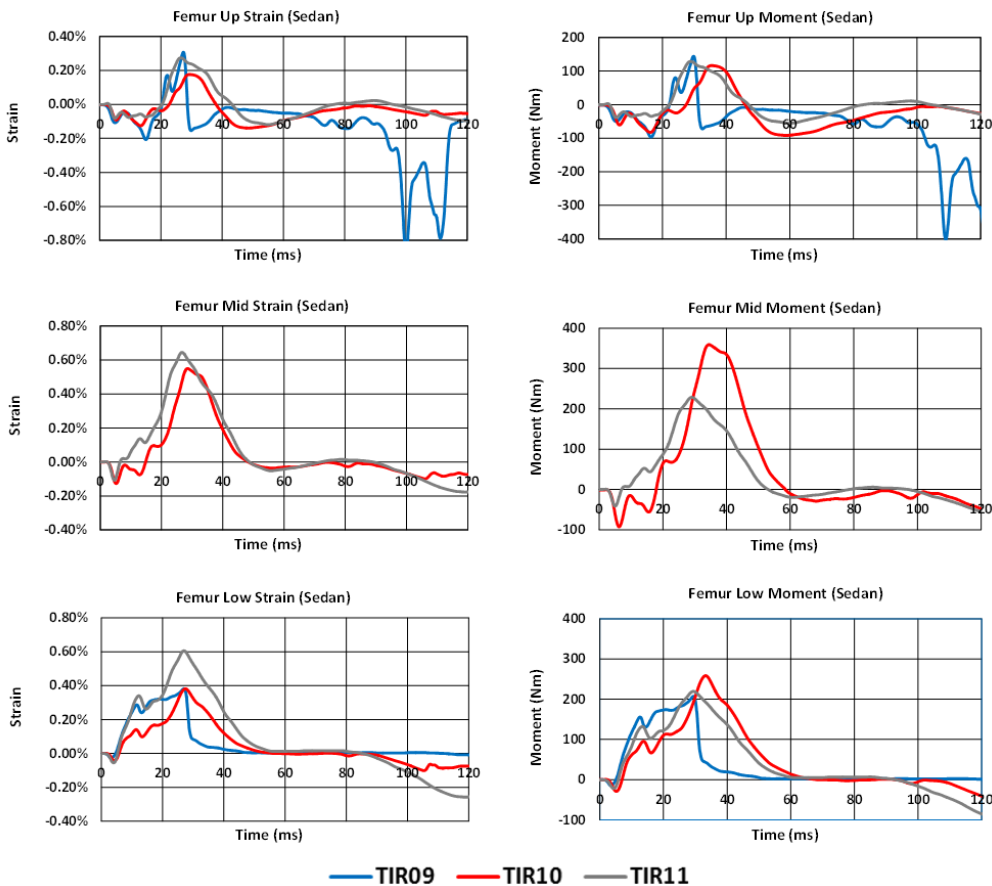


Fig. 7. PMHS responses in the Sedan configuration: raw femur strain measurements (left column), femur cross-section moments derived and scaled to the 50<sup>th</sup> percentile male (right column).

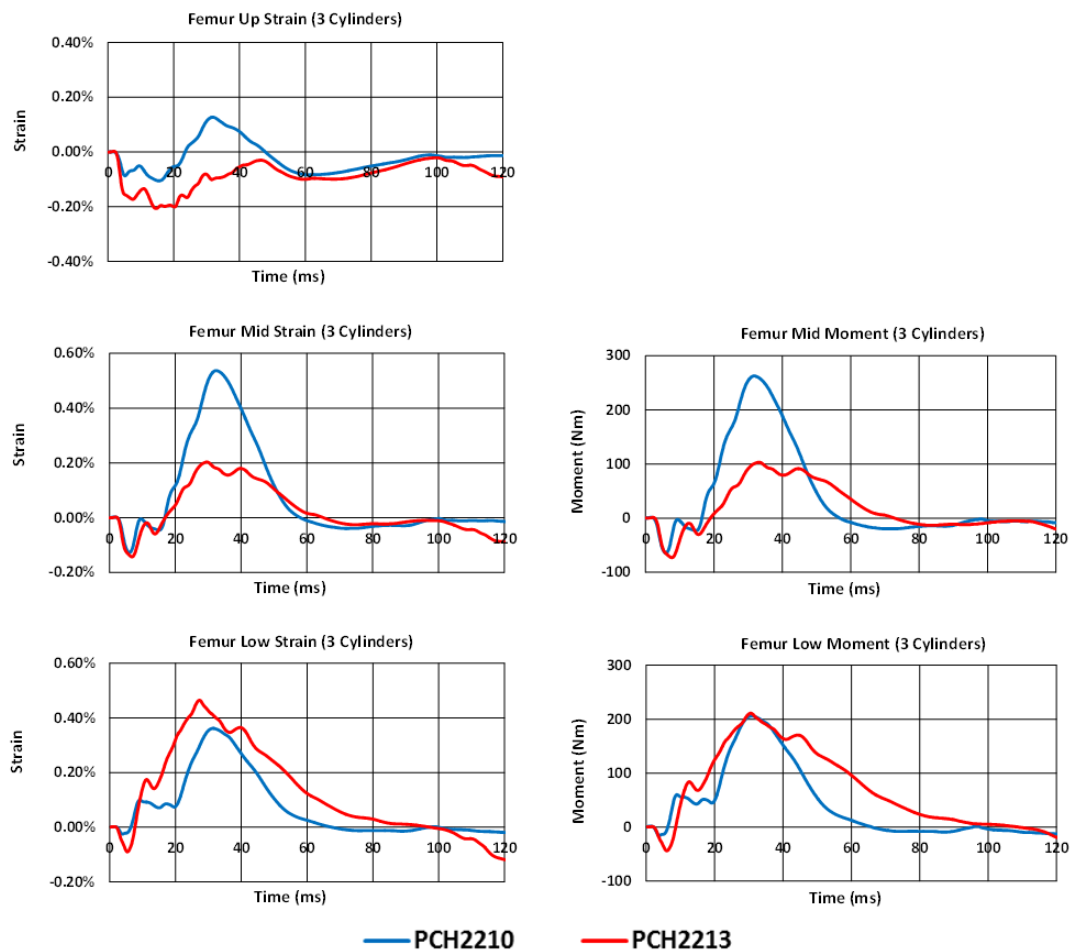


Fig. 8. PMHS responses in the 3 Cylinders configuration: raw femur strain measurements (left column), femur cross-section moments derived and scaled to the 50<sup>th</sup> percentile male (right column).

#### IV. DISCUSSION

There are few experimental data in literature relating to femur cross-section moments in full-scale PMHS pedestrian tests. However, these moments are used as injury criteria to assess pedestrian protection. The current study provided this type of data, making it possible to evaluate biofidelity of HBMs, physical dummies and lower extremity impactors regarding femur moment prediction.

A considerable effort was taken to acquire this type of data in this study. On one hand, strain gauges were installed on the femurs of the PMHS used in the full-scale pedestrian impact tests and, on the other hand, these femurs were isolated from the PMHS after the full-scale tests and were submitted to three-point bending tests. By coupling these two types of test, femur moments were derived and corridors were established for four vehicle configurations.

However, the above approach exhibited some limitations. First, the quasi-static three-point bending tests did not capture the strain rate effects on strain-moment relationship in dynamic pedestrian tests. From this point of view, the moments in the femur may be underestimated. No available data allowed the authors to quantify this effect.

Another limitation of this approach is related to the difference in boundary condition of the thigh in a full-scale car-pedestrian impact with respect to the three-point bending tests on isolated femurs. Indeed, the femur in three-point bending test is subjected to bending only, while tensions or compression were superimposed to the bending in the full scale test. Simulations of the full scale PMHS tests with the GHBMCM50-PS pedestrian model were first run to evaluate if the contribution of the tension-compression in the strain is negligible compared to the contribution of the bending. Figure 9 show the total strain and the component strain due to tension and compression in the right femur. It can be observed that the strain generated by the tension and

compression represented less than 7% of total strain for the SUV, 3% for the Van and, 1% for the Sedan. So the inaccuracy of the approach used in this study seems to be very limited.

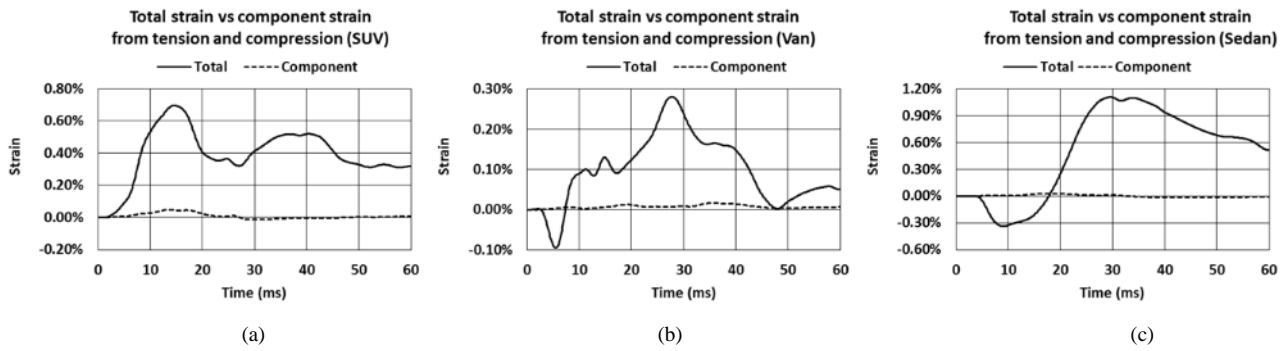


Fig. 9. Contribution of the tensile and compressive force to the total mid femur strain in the full scale PMHS tests for the SUV, Van and Sedan configurations, estimated using GHBM simulations.

It is also to be noted that the loading direction was purely lateral-to-medial in the three-point bending tests, while it may not be exactly the case in the full scale tests. To estimate the influence of this difference on the estimation of the moment, the right femur of the GHBM M50-PS was extracted and was loaded in three-point bending, first in purely lateral-to-medial direction (noted as 0°), then the femur was rotated by +20° and by -20° and was loaded in the same condition. Figure 10 compares the moment-strain relationships corresponding to these three loading directions. They are almost identical with an angle of +20° and an angle of -20°. The variation with an angle of 0° and an angle of ± 20° is less than 3%.

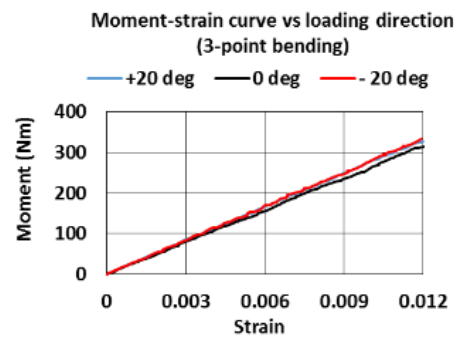


Fig. 10 Influence of the loading direction on the moment strain relationship in the three-point bending simulation with the GHBM M50-PS right femur model.

It is possible that the femur moments were overestimated to some extent in this study. In fact, these femurs were already loaded in the full-scale pedestrian tests, and some of them submitted plastic deformation at some measurement locations. For these cases, the moment-strain relationship beyond the elastic threshold was stiffer in the three-point bending tests than in the full-scale pedestrian tests. It is also to be noted that the femurs taken from the PMHS tested were only examined in macroscopic level to assure its appropriateness for three-point testing. However, a potentially damaged bone, with alteration of its micro-structures, might become less stiff. In this case, the derived moments might be underestimated. Further investigation is needed to know which one of the above two considerations is more relevant.

In tests TIR03 and TIR09, the right femurs fractured. Consequently, it was impossible to perform three-point bending tests to acquire the corresponding strain-moment relationship for these two femurs. The only solution was to approximate this relationship by performing three-point bending tests on the left femurs. In order to assess difference between the left and right femurs in terms of moment-strain relationship, three-point bending tests were carried out for both the left and the right femurs with PMHS MS700 and MS701. Figure 11 and Table VI show the response difference, which rose up to 29% in the worst case.

TABLE VI

VARIATION OF THE ELASTIC MODULUS IN THE MOMENT-STRAIN RELATIONSHIP BETWEEN THE LEFT AND RIGHT FEMURS AND BASED ON THREE-POINT BENDING TESTS WITH PMHS MS700 AND MS701

	MS700_SUV TIR04			MS701_SUV TIR5		
	Low	Mid	Up	Low	Mid	Up
Left femur	363	330	360	502	433	472
Right femur	281	312	413	442	395	384
Left/Right	29%	6%	-23%	14%	9%	23%

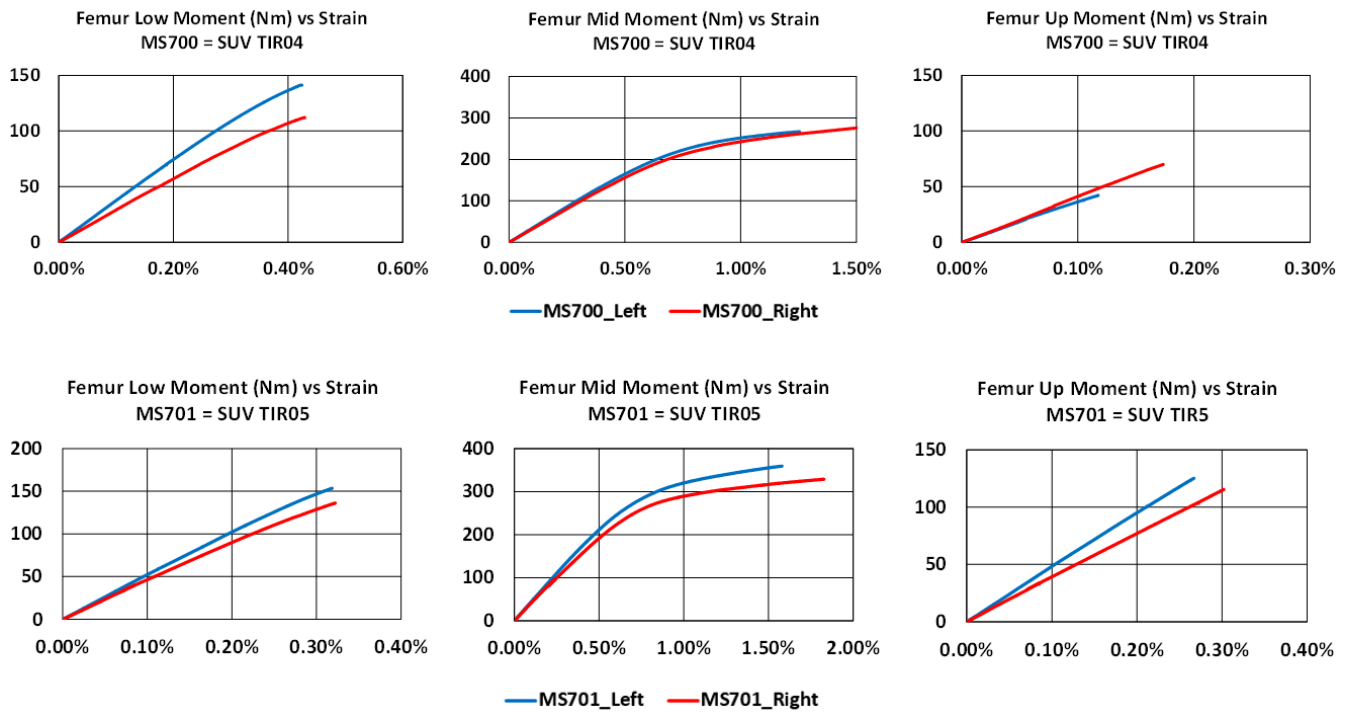


Fig. 11. Response difference between the left and right femurs in terms of moment-strain relationship and based on three-point bending tests with PMHS MS700 and MS701.

It was observed that the peak strain in the three-point bending test was less than that in the full scale PMHS tests. This happened mainly for the upper strain. The reason is that the strain gauge at the upper location was close to the supporting point so the lever arm was small and limited development of moment and strain. In the full scale test, the lever arm was more important due to the presence of the femur neck and head. Two exceptions were the mid strain for tests TIR01 and TIR02. A hypothetical explanation may be that the femurs were weakened in the full-scale tests.

**V. CONCLUSIONS**

A new method was developed to estimate cross-section moments in the femur in full-scale PMHS pedestrian tests. It consisted of coupling the femur strains measured in a full-scale PMHS pedestrian test and the moment-strain relationships delivered by a three-point bending test on the same femur.

Cross-section moments in three locations of the femur were estimated for four series of full-scale PMHS pedestrian tests, and corresponding biofidelity corridors were established.

Strains in three locations of the femur were also provided.

**VI. ACKNOWLEDGEMENTS**

The authors would like to acknowledge the donors, whose generosity allowed this study to be carried out. The contributions of Denis Dubois, Catherine Potier and Pascal Baudrit from CEESAR are also greatly appreciated.

**VII. REFERENCES**

[1] Kajzer, J., Schroeder, G., Ishikawa, H., Matsui, Y., Bosch, U. (1997) Shearing and bending effects at the knee joint at high speed lateral loading. *Stapp Car Crash Conference*, **41**: pp. 151–65.

- [2] Bose, D., et al. (2004) Response of the knee joint to the pedestrian impact loading environment. *SAE 2004 World Congress*, SAE Technical Paper #2004-01-1608.
- [3] Kerrigan, J. R., et al. (2005) Kinematic Corridors for PMHS Tested in Full-Scale Pedestrian Impact Tests. *Proceedings of the 19th International Technical Conference on the Enhanced Safety of Vehicles (ESV)*, 2005, Paper 05-0394.
- [4] Kerrigan, J. R., Crandall, J. R., Deng, B. A. (2008) Comparative Analysis of the Pedestrian Injury Risk Predicted by Mechanical Impactors and Post Mortem Human Surrogates. *Stapp Car Crash Journal*, **52**: pp. 527–67.
- [5] Forman, J. L., et al. (2015) Biofidelity corridors for whole-body pedestrian impact with a generic buck. *Proceedings of the IRCOBI Conference*, 2015.
- [6] Song, E., et al. (2017) New Reference PMHS Tests to Assess Whole-Body Pedestrian Impact Using a Simplified Generic Vehicle Front-End. *Stapp Car Crash Journal*, **61**.
- [7] Song, E., et al. (2017) Reference PMHS Tests to Assess Whole-Body Pedestrian Impact Using a Simplified Generic Vehicle Front-End. *Proceedings of IRCOBI Conference*, 2017.
- [8] Untaroiu, C. D., Putnam, J. B., Schap, J., Davis, M. L., Gayzik, F. (2015) Development and Preliminary Validation of a 50<sup>th</sup> Percentile Pedestrian Finite Element Model. ASME. International Design Engineering Technical Conferences and Computers and Information in Engineering Conference, Volume 3: 17th International Conference on Advanced Vehicle Technologies; 12th International Conference on Design Education; 8th Frontiers in Biomedical Devices: V003T01A004. doi:10.1115/DETC2015-47781.
- [9] Mizuno, Y. (2005) Summary of IHRA Pedestrian Safety WG Activities (2005) – Proposed Test Methods to Evaluate Pedestrian Protection Afforded by Passenger Cars. *Proceedings of the 19th International Technical Conference on the Enhanced Safety of Vehicles (ESV)*, 2005, Paper 05-0138.
- [10] SAE International (2010) Performance Specification for a Midsize Male Pedestrian Research Dummy. *SAE International, Surface vehicle Information Report J2782 OCT2010*.

**VIII. APPENDIX**

Figures A1-A4 below provides femur moment-strain relationships given by three-point bending tests (black curves). The relationship beyond a strain level of 0.8% were not presented since the peak strains measured in the full-scale tests did not exceed 0.8%. In order to show how good the bilinear elastoplastic model (composed of a first part with an elastic modulus until a strain of 0.5% and a second part with a tangent modulus of 2400 Nm/strain beyond 0.5%) was to approximate the experimental data, the moment-strain relationships established with the model (dotted curves) were compared to those measured experimentally (solid curves). The dotted curves should not be considered as the effective moment-strain relationships used to derive the moment in the full-scale tests. It's to be recalled that this bilinear elastoplastic model was used only for 4 tests (TIR01-04) at its upper femur strain measurement locations (corresponding to red cells in Table IV, as explained in the “femur moment calculation for full-scale pedestrian tests” section).

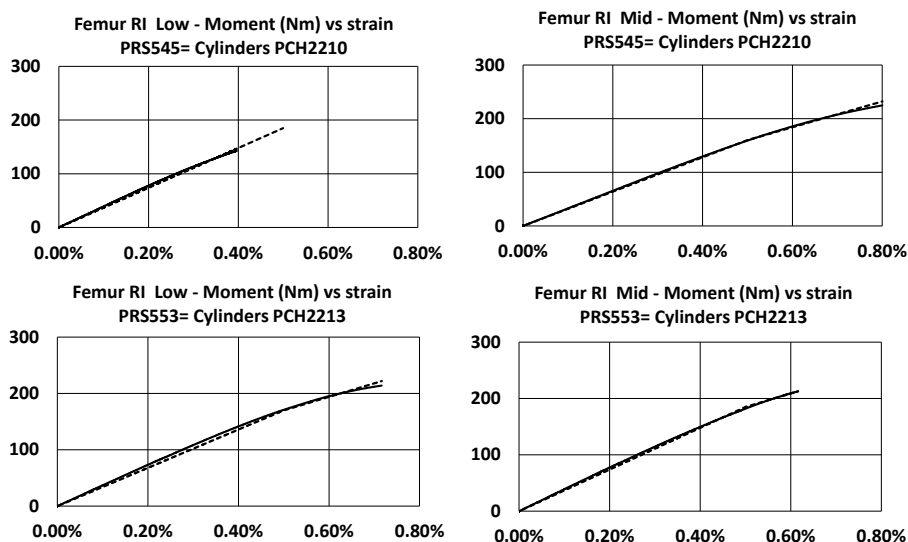


Fig. A1. Femur moment-strain relationships given by three-point bending tests for the 3 Cylinders configuration (solid curves) and approximated by bilinear elastoplastic models (dotted curves).

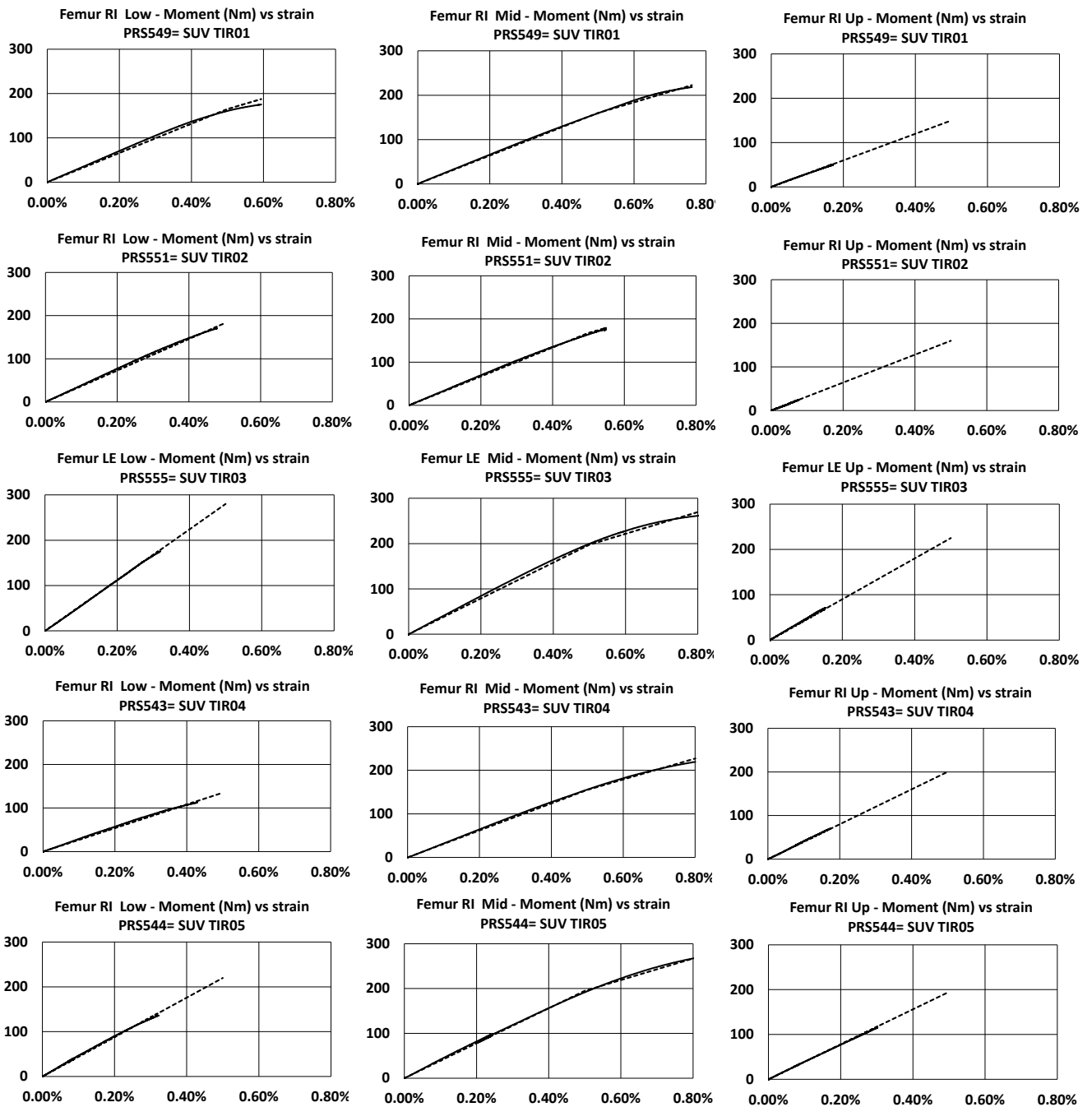


Fig. A2. Femur moment-strain relationships given by three-point bending tests for the SUV configuration (solid curves) and approximated by bilinear elastoplastic models (dotted curves).

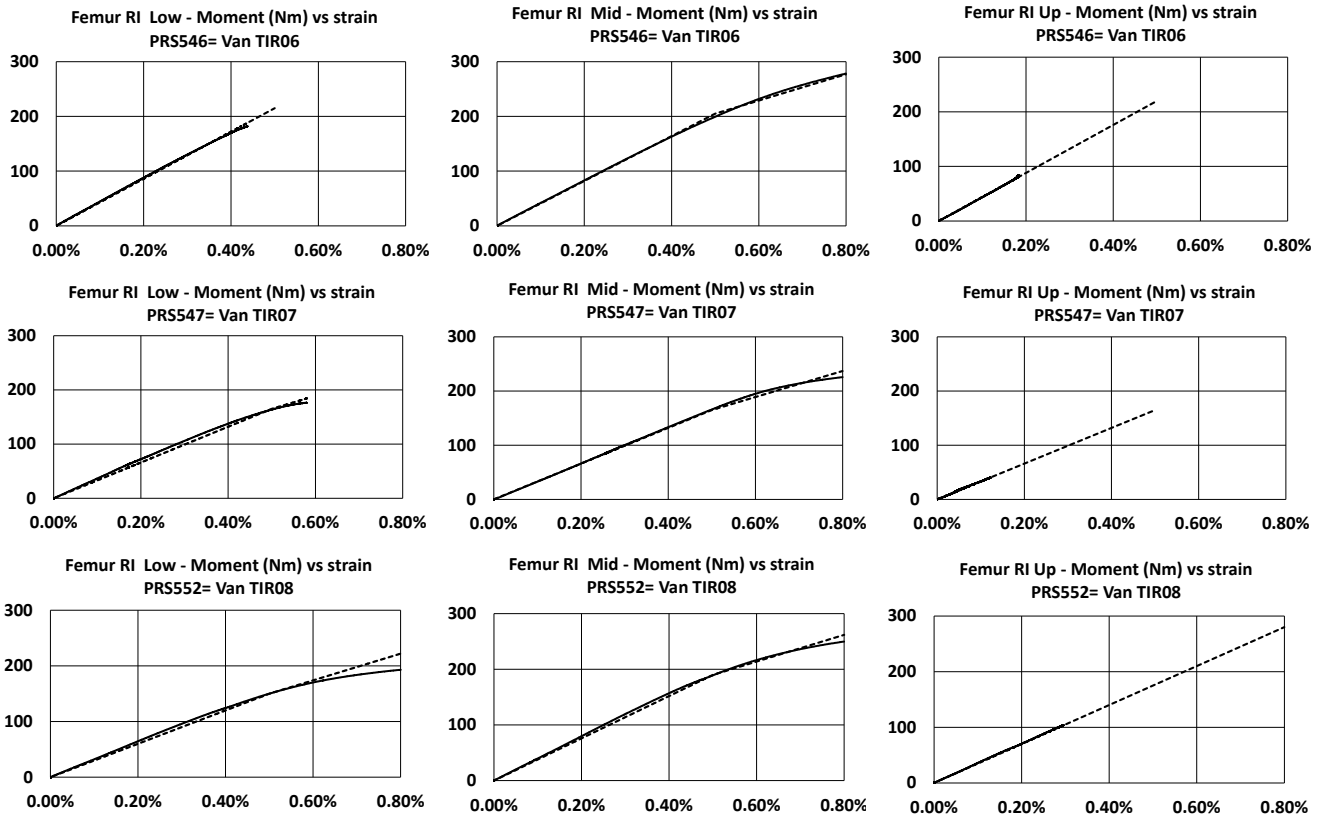


Fig. A3. Femur moment-strain relationships given by three-point bending tests for the Van configuration (solid curves) and approximated by bilinear elastoplastic models (dotted curves).

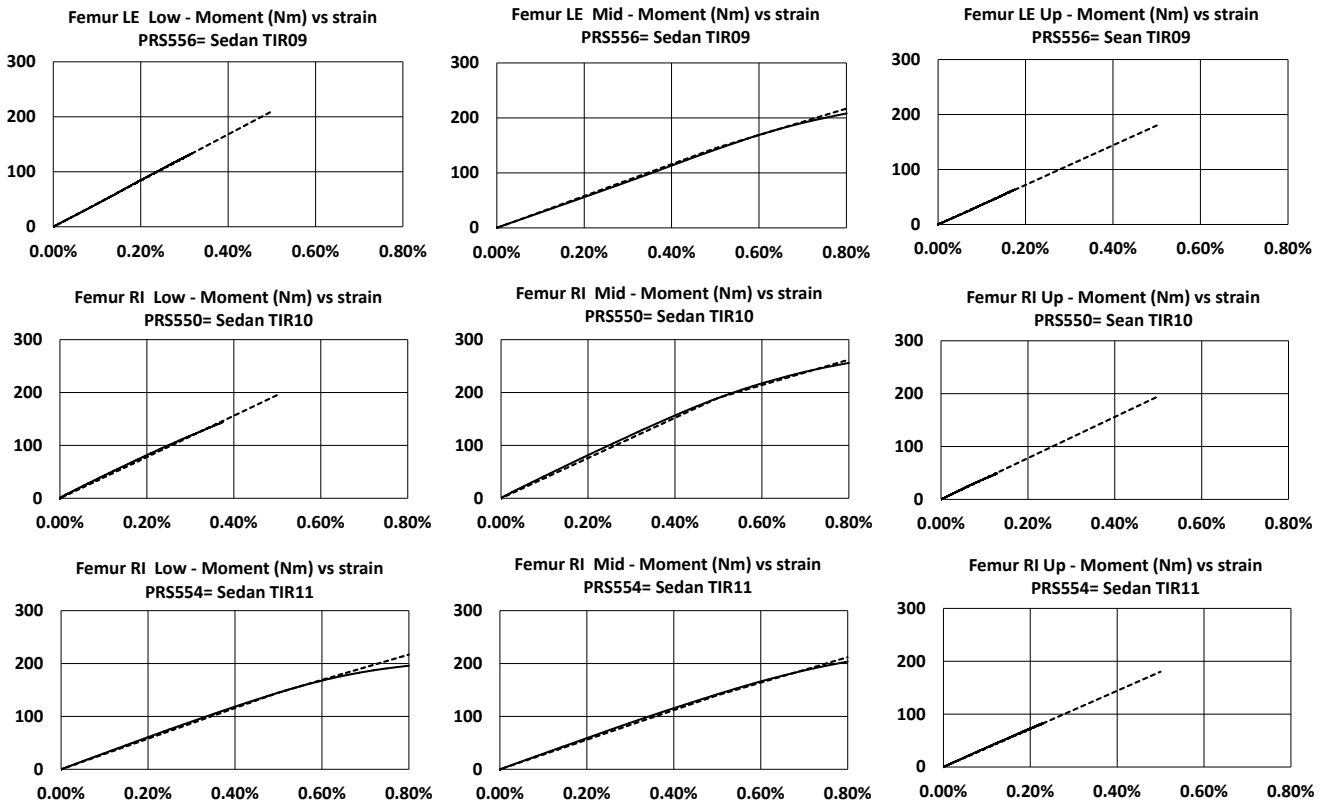


Fig. A4. Femur moment-strain relationships given by three-point bending tests for the Sedan configuration (solid curves) and approximated by bilinear elastoplastic models (dotted curves).

TABLE A-I  
 SUPPLEMENTARY DATA FOR THE THREE-POINT BENDING TESTS WITH NORMALISED RELATIVE GAUGE POSITIONS, SPAN LENGTH AS WELL AS PEAK STRAINS AND LOADING FORCES

Test #	Peak force (N)	Peak strain (Low)	Peak strain (Mid)	Peak strain (Up)	Span length (mm)	Norm. L1 (Support)	Norm. L2 (Pivot)	Norm. L3 (Gauge Up)	Norm. L4 (Gauge Mid)	Norm. L5 (Gauge Low)
PRS549	435	0.59%	0.76%	0.17%	284	-0.50	0.50	-0.42	-0.15	0.22
PRS551	352	0.49%	0.55%	0.08%	316	-0.50	0.50	-0.46	-0.18	0.19
PRS555	414	0.32%	0.81%	0.15%	325	-0.50	0.50	-0.40	-0.11	0.24
PRS543	433	0.43%	1.91%	0.17%	272	-0.50	0.50	-0.38	0.00	0.31
PRS541	421	0.42%	1.26%	0.12%	275	-0.50	0.50	-0.43	-0.04	0.25
PRS544	463	0.32%	1.83%	0.30%	294	-0.50	0.50	-0.33	-0.02	0.30
PRS542	516	0.32%	1.58%	0.27%	288	-0.50	0.50	-0.33	-0.02	0.30
PRS546	473	0.44%	2.13%	0.18%	342	-0.50	0.50	-0.40	-0.01	0.27
PRS547	350	0.58%	1.11%	0.12%	342	-0.50	0.50	-0.43	-0.10	0.21
PRS552	414	0.88%	1.63%	0.30%	330	-0.50	0.50	-0.35	-0.07	0.21
PRS556	385	0.32%	1.15%	0.18%	325	-0.50	0.50	-0.40	-0.07	0.29
PRS550	351	0.37%	0.84%	0.13%	325	-0.50	0.50	-0.41	-0.04	0.25
PRS554	408	1.14%	2.22%	0.23%	332	-0.50	0.50	-0.38	-0.08	0.18
PRS545	392	0.40%	1.78%	0.02%	342	-0.50	0.50	-0.47	-0.07	0.29
PRS553	387	0.72%	0.62%	0.05%	331	-0.50	0.50	-0.47	-0.17	0.17

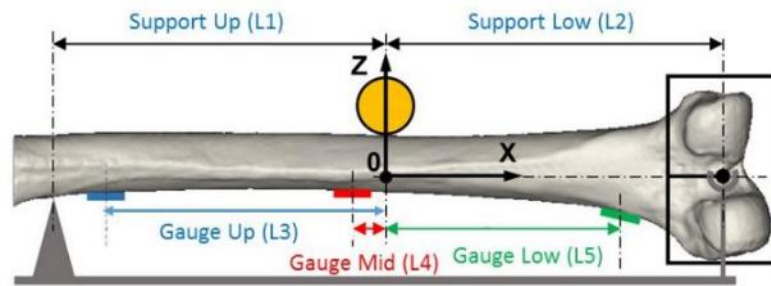


TABLE A-II  
 NORMALISED LOCATIONS OF FEMUR GAUGES SHOWING VARIABILITY BETWEEN SUBJECTS

Subject	Femur low	Femur mid	Femur up
MS697	76%	51%	34%
MS698	74%	49%	28%
MS699	78%	56%	35%
MS700	80%	59%	35%
MS701	80%	59%	37%
MS712	78%	58%	30%
MS708	74%	52%	28%
MS707	74%	55%	33%
MS711	81%	55%	32%
MS710	76%	56%	29%
MS709	72%	51%	29%
<b>Average</b>	<b>77%</b>	<b>55%</b>	<b>32%</b>
<b>St. Dev</b>	<b>3%</b>	<b>3%</b>	<b>3%</b>